# POLITECNICO DI TORINO
## Repository ISTITUZIONALE

Physical and mechanical properties of a reversible adhesive for automotive applications

(Article begins on next page)

23 April 2024

# Physical and mechanical properties of a reversible adhesive for automotive applications☆

R. Ciardiello[a,*], G. Belingardi[a], B. Martorana[b], V. Brunella[c]

[a] Politecnico di Torino, Department of Mechanical and Aerospace Engineering, Corso Duca degli Abruzzi 24, 10129 Torino, Italy
[b] Centro Ricerche Fiat S.C.p.A., Group Materials Labs, Corso Settembrini 40, 10135 Torino, Italy
[c] Department of Chemistry and NIS Research Centre, University of Torino, 10125 Torino, Italy

## ARTICLE INFO

## ABSTRACT

In this work, a hot-melt adhesive used by automotive industries for bonding plastic components has been modified with three different percentages of nanofiller (iron oxide) in order to make the adhesive electromagnetically sensitive and to perform adhesive joint separations. $Fe_3O_4$ particles with a weight concentration of 3%, 5% and 10% were embedded in the adhesive matrix. Single Lap Joint (SLJ) tests showed that a slight increase of the maximum load and a more ductile behaviour are obtained. The sensitivity of these modified adhesive performance to the induction heating process was studied with respect to some relevant parameters: the current (or power), the frequency of the electromagnetic induction field and the shape of the coil. Furthermore, the diameter of the hollow copper coil was modified in order to understand whether the coil temperature has an effect on the separation time. The separation time, that is an index of the time needed to reach the melt of the adhesive and the consequent SLJ separation, together with the temperature profile of the adhesives have been used to evaluate the sensitivity of these adhesives to the process parameters. The analysis on the temperature and separation time showed that the most influencing parameter is the frequency of the electromagnetic induction field. As expected, also the shape of the coil influences the separation time, in particular, the adhesive joint separated with the pancake coil showed lower values of the separation time compared to the solenoidal coils. Scanning Electron Microscope (SEM) showed that iron oxide particles tend to form small agglomerate that resulted well dispersed in the adhesive matrix. Thermogravimetric analysis (TGA) was used to verify that the separation procedure do not degrades these modified adhesives.

## 1. Introduction

In recent decades, the use of the adhesive bonding is widely increased in many industrial sectors. In the automotive field, the light-weight construction strategies find great advantages from the use of adhesives. Adhesives represent a lighter and cheaper solution, in some cases, with respect to traditional fasteners. They permit to join parts made of materials that are difficult or even impossible to join in other ways and they permit to join substrates made of different materials (hybrid structures). Other advantages of adhesive bonding, reported in [1–4], include reduction of vibration and noise damping, insensitivity to some corrosive environments, direct and indirect reduction in join weight, high mechanical performance, better stress distributions, easiness of the joint fabrication and the possibility to increase the stiffness without weight addition.

Although they offer a wide range of advantages, some issue can limit their use, such as open time and the complexity to dismantle joints without introducing damages to the substrates. Open time is the time that can be used for the application of the adhesive and to the application of the bonding pressure in order to obtain an acceptable adhesion. In the case of thermoplastic adhesives, open time can be very short. The open time of the adhesive used in this work is around 30 seconds, thus the time to couple two components is limited. Traditionally, as reported by Lu et al. [5], components that are bonded with hot-melt adhesives (HMA) can be separated by warming the adhesive up to its melting temperature, by the mechanical cut of the adhesive layer or by the use of a chemical solvent. Unfortunately, in the first case, the melting temperature of the HMA can be close to the melting temperature of the plastic substrates, and the disassembly process can introduce severe damages to the substrates. The same can

---

be told for the process based on the mechanical separation of the adhesive. They can lead to damages of substrates, due to the non-uniform shape of the bondline and moreover, at times, the bondline is not visible but well integrated into the structures and the only possible way to separate the components is breaking them. This separation methodology refers especially to these applications. On the other hand, the chemical dissolution of the adhesive can be only used in rare occasion since the solvent can be aggressive for the components as well. Lu et al. [5] report rather laborious mechanical and chemical systems able to separate adherends, but these methods have two typical drawbacks: the surfaces are not clean at the end of the process and the possibility to introduce damages to the substrates is likely. Furthermore, these systems are extremely complex to be adopted in mass production. For these reasons, a more efficient system has to be found in order to achieve the disbonding of substrates without introducing damages to the adherends.

Recently, some innovative technologies have been studied in order to set a viable solution to these problems. Verna et al. [6], Banea et al. [7] and Ciardiello et al. [8] have presented a technology that uses electromagnetic induction process in order to activate magneto-sensitive nanoparticles embedded in HMA adhesives. The sensitivity of these particles to the electromagnetic field allows a relatively rapid increase of adhesive temperature and thus the possibility to bond and separate adherends with greater easiness and without damages. Severijns et al. [9] have used the same technology for curing epoxy adhesives.

In electromagnetic induction process, an inductor is used to increase the temperature of a workpiece, usually a metallic component. Inductor works as a primary of an electric transformer and conductive material as a secondary one. The electromagnetic field is generated by a coil that is the final element of the inductor and the shape of the electromagnetic field is given by the shape of the coil. The coil is fabricated with a hollow copper tube with water that flows inside to refrigerate the coil itself. The temperature increase of the particles is mainly due to the hysteresis losses and the Neel and Brown relaxation phenomena that are well explained in [10–13]. It is strictly linked to the dimension of the nanoparticles, in fact, particles with size smaller than 50 nm exhibit superparamagnetic behaviour that leads to a more rapid increase of the temperature, as Ghazanfari et al. [11] have reported.

The motivations of this study are due to the lack of information on this topic and to the different sensitivity and behaviour of the nanoparticles compared to metal workpieces. While induction heating coupled with metal component has been widely studied [14,15], the induction heating process coupled with magnetic nanoparticles embedded in the adhesive is at an early stage. This latter process is based on properly shaped inductor coils and properly set electromagnetic field control unit.

In this work, the sensitivity to some process parameters, in the case of the magnetite nanoparticles dispersed in the HMA, has been studied. The HMA used in this work is used to bond plastic components in automotive industries, such as rear tail gates, plastic bumpers, air ducts for conditioning system, housing assemblies of lamps and some aesthetic skins. An example of an automotive component bonded with this adhesive is the low tail gate of the rear door that is shown in [16]. The parameters investigated are the shape of the coil, the frequency of the generator and the circulating currents in the coil. Furthermore, the three diameter of the pipe coil were investigated in order to investigate the temperature increase of the coils themselves that, at some temperatures, could influence the heating processes. Two different shapes of the coil were chosen in order to assess the sensitivity of nanomodified adhesive to two different electromagnetic fields. The separation tests with different diameters of the pipe coil were carried out to assess whether the different diameter of the pipe coil, linked to the water mass flow and to the coil temperature can affect the separation process. Finally, the separation tests were carried out at different values of currents (power) and frequencies of the magnetic field in order to evaluate the sensitivity of these nanomodified adhesives to these factors. The
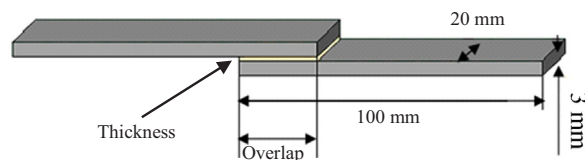


**Fig. 1.** Main dimensions of the single lap joint specimen.

parameters used to measure this sensitivity is the time needed to separate a single lap joint specimen and the temperature (SLJ). The thermoplastic adhesive was modified with three different weight concentrations of iron oxide particles, namely 3%, 5% and 10%. The aim was to investigate the possibility to separate modified adhesives with relatively low-weight particle concentrations and to study the effect of the particle weight percent on the separation time and the temperature-time curve.

## 2. Materials and methods

Experimental tests were conducted on Single Lap Joint (SLJ) specimens, shown in Fig. 1, for both mechanical and separation tests. The mechanical properties of this adhesive were already studied in [17–19]. Koricho et al. [17] have studied the effect of overlap length and of adhesive layer thickness. Ciardiello et al. [18,19] have studied the effect of the ageing effects and impact responses of this pristine and nanomodified adhesives as well. Fig. 1 shows the dimensions of the substrates and the joint, in particular, the adhesive layer thickness and the overlap length was set equal to 1 mm and 25 mm, respectively.

The joints used for the experimental tests were obtained by bonding substrates made of a polypropylene copolymer with 10% in weight of talc (Hifax CB 1160 G1, by Lyondell-Basell Industries). The substrates were bonded with a polyolefin-based HMA (Prodas, by Beardow Adams) a copolymer of polypropylene and polyethylene. The nanomodified adhesives were prepared by using a hot plate for melting the pristine adhesive and by adding iron oxide particles with an average size smaller than 50 nm ($Fe_3O_4$, by Sigma-Aldrich) with three different weight concentrations (namely 3%, 5% and 10%). The choice of these particles size was due to the fact that the iron oxide particles with this size exhibit a superparamagnetic behaviour because of their particles dimensions. The adhesive and the nanoparticles were mixed together by means of a glass rod. Following a procedure commonly adopted in the literature for HMAs, pellets were melted together at 190 °C, using the hot plate. At 190 °C, the viscosity of the adhesive is low enough to easily mix the particles into the adhesive by mean of a glass rod. The iron oxide nanoparticles were added gradually and mixed together with the adhesive for 10 minutes. A mechanical, thermal and chemical characterisation of this pristine adhesive can be found in Koricho et al. [17]. The main values are reported in Table 1. The values related to the melting point were evaluated by a Differential Scanning Calorimetry analysis (DSC). The DSC curves presented two peaks, at 124 °C and 155 °C, due to the presence of two polymers, polypropylene, and polyethylene [17].

Tensile tests were carried out on the substrate at 100 mm/min, which is the same speed of the SLJ tests. This rate was chosen according to the Fiat Chrysler Automobile (FCA) standard on hot melt adhesive, already used in [3,8,17]. The mechanical tests were conducted using an Instron 8801. Two tabs were attached to the extremities in order to

**Table 1**
Physical properties of the hot-melt adhesive.

| Melting temperature(Initial - Final) | 124 °C − 155 °C |
|---|---|
| Viscosity at 180 °C (S. 27/5 rpm) (BA QA102) | 22 – 28 Pa*s |
| Open time | 30 s |
| Density | 0.98 g/cm$^3$ |
| Initial thermal degradation temperature | 210 °C |

**Table 2**
Mechanical properties of the substrates.

| Initial yield (MPa) | Max. tensile stress (MPa) | E (GPa) | $\nu_{elastic}$ |
|---|---|---|---|
| 15.1 | 20 | 1.90 | 0.4 |

avoid the misalignment of the SLJ tests. The main properties of the substrates are reported in Table 2. Five replications were carried out for all the mechanical tests.

Each substrate was cleaned with isopropyl alcohol in order to remove possible residuals from the specimen before the joints preparation. The joint preparation was performed with a hot-melt gun (Fig. 2a) and an assembly device (Fig. 2b) which permits the regulation of the adhesive thickness joint. The most part of the tests was performed on SLJ specimens with 1 mm of nominal thickness. The use of this thickness was determined by the analysis of the tolerances of a bonded real plastic bumper. However, the effect of three different thicknesses (0.5 mm, 1 mm and 1.5 mm) was analysed as well. The used adhesive layer thickness is 1 mm, the typical value recommended by the supplier of this adhesive and adopted by the automotive industry.

The bonding procedure was performed in the following steps. As shown in Fig. 2, the substrate (lower substrate in Fig. 2b) is fixed on the lower base of the assembly device. The HMA at high temperature (190 °C) was uniformly spread through the hot melt gun over the lower substrate. Finally, the upper substrate (upper substrate in Fig. 2b) was placed on the hot adhesive. In order to ensure the squeezing of the melted adhesive and guarantee a better adhesion strength, a pressure was applied by means of weights (3.5N) placed on the upper substrate. The thickness of each joint was measured and it was found to be constant along the joint length, with a variation smaller than 0.03 mm.

Fig. 3 shows the typical configurations of the test and the coil shape used in this work. On the left side, the Fig. 3a shows the circular three-turn coil. In this configuration, the SLJ specimen is placed at the centre of the coil, along with the vertical direction. Fig. 3b shows a three-turn elliptical shape coil. This configuration was chosen in order to understand whether the closeness of the coil to the adhesive layer can give better performance when compared to the previously adopted circular coil. The internal diameter of the circular coil is 25 mm so the distance between the internal diameter of the coil and the substrate is 9 mm on both sides. On the other hand, the minor axis of the elliptical coil is 17 mm (the distance between the internal diameter of the coil and the substrate is 5 mm on both sides), the major axis is 26 mm. Fig. 3c shows the pancake coil which is more attractive for industrial applications and processes because it can be easily placed and moved over the area of interest, approaching the joint from one side and giving also the opportunity to control easily the distance of the inductor from the workpieces. The circular and the elliptical coils (solenoids) generates a similar electromagnetic field that is different compared to the pancake

coil. For each test, a weight of 0.5 N was applied to the lower substrate of the SLJ in order to submit the joint to a constant load and cause joint separation (by part sliding) when the adhesive reached its melting temperature. In the case of the pancake, a pulley was used because the experimental test was conducted in the horizontal position. The results presented in the next section refer the average separation time calculated on five replications.

The two different fields are shown in Fig. 4. The left side of the Figure shows the field generated by a solenoid. As illustrated, the field is more intense in the centre of the coil. The right part of the Figure shows the middle section of the pancake coil and its electromagnetic field. In this case, the electromagnetic field is more intense in the centre as well but the workpiece can be placed over the coil with any special requirement about the dimension. On the other hand, the solenoid has to be large enough to house the workpiece and larger coils have a low frequency that is a high influencing parameter as it has been shown in this work.

The generator used for this analysis was Easyheat by Ambrell, with a maximum power of 10 kW and a frequency range from 10 to 400 kHz. All the manufactured coils presented a constant diameter and sectional area. The operational frequency of the system is automatically calculated by the system and depends on the length, the number of turns and the diameter of the coil.

Thermogravimetric analyses (TGA) were carried out on a TA Q500 model from TA Instruments by heating samples contained in alumina pans at a rate of 10 °C/min from 50 to 600 °C in nitrogen atmosphere. The instrument records the weight and the weight loss rated with the temperature increment as a function of the temperature.

Scanning electron microscope (SEM) analysis was carried out using a Carl-Zeiss EVO50. An electronic high tension of 20 kV was used together with secondary emission signal. The specimens were properly coated with gold in order to have better images.

## 3. Results and discussion

In this section, the mechanical results and dependency of the induction heating process on the nanomodified adhesive were investigated. The results of SLJ tests are presented. In particular, the dependency of separation time on the applied current, frequency, shape and tube diameter is analysed. Thermo-gravimetric analysis and scanning electron microscope images were reported as well.

*Nomenclature*.

In the following sections, HMA is referring to the pristine hot-melt adhesive, HMA_3%, HMA_5%, and HMA_10% are referring to the adhesive modified with the 3% wt., 5% wt. and 10% wt. of iron oxide, respectively.
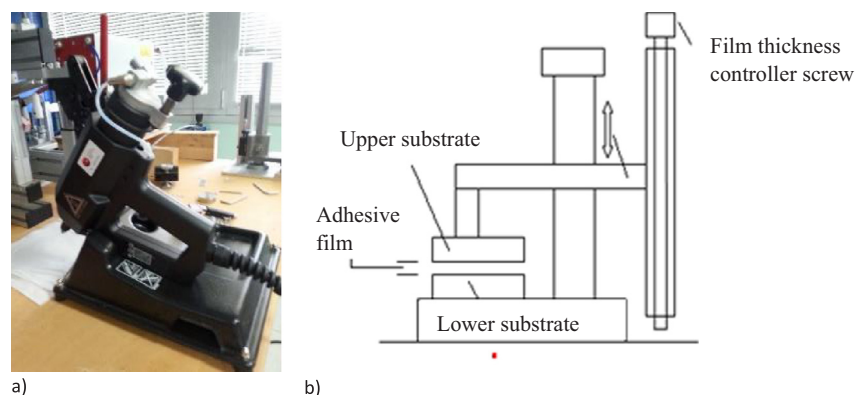


a)                    b)

**Fig. 2.** Instrumentation used for the joint preparation: a) hot melt gun; b) assembly device [17].
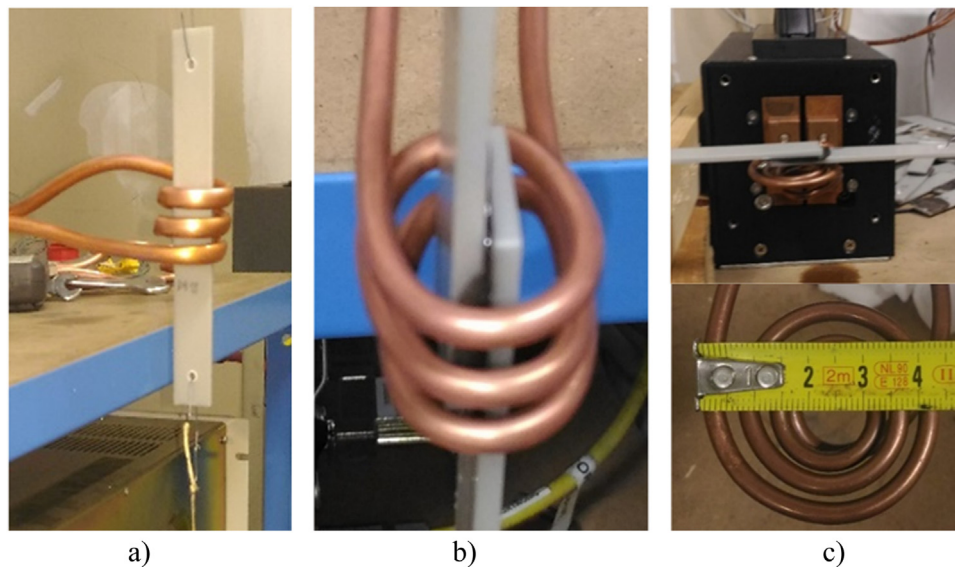
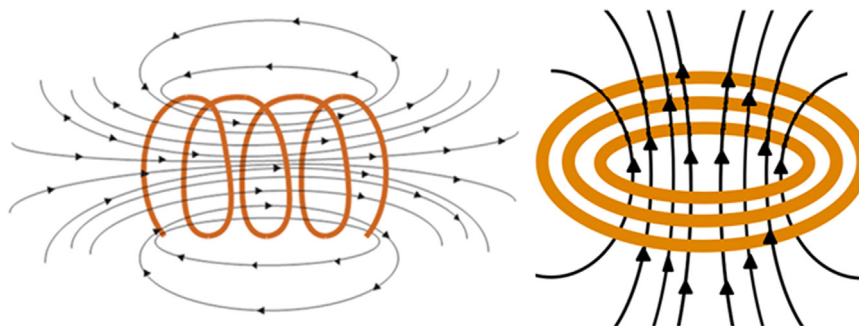**Fig. 3.** Circular coil a), elliptical coil b) and pancake coil c) adopted for the experimental tests.



**Fig. 4.** Electromagnetic fields of the studied coils.

### 3.1. Mechanical tests

Fig. 5 shows the typical trends of SLJ tests for all the four different adhesive formulations. The curves are relative to the SLJ tests with an overlap of 25 mm and an adhesive layer thickness of 1 mm. The pristine HMA is the black curve that is the lowest curve in the diagram. As illustrated, the increase of the particles content brings to an increase of the adhesive shear strengths and to a more ductile behaviour of the modified HMAs, as can be noted by the larger tails on the right part. The nanomodified adhesives have larger elongations compared to pristine HMA as well. Mechanical properties of HMA_3% and HMA_5% are very clos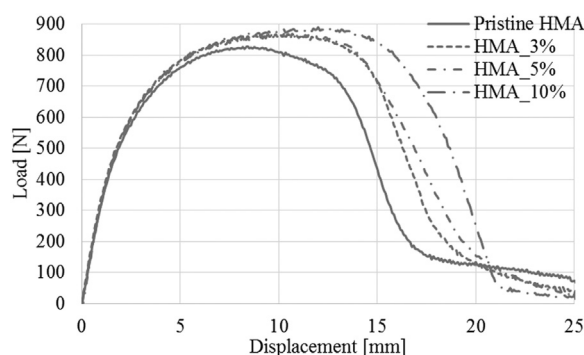e. As can be noted the initial parts of the curves are superimposed for all the adhesive compositions. The increase of the maximum loads of the nanomodified adhesives could be due to the microagglomerates that are shown in the SEM section. These agglomerates lead to a toughening of the bondline that resulted in an increase of the maximum shear strength as explained in [6,20].

Table 3 reports the average maximum shear strength values. The Table illustrates that there is a percentage increase of 5.1%, 5.5% and 7.2% over the pristine adhesive for HMA_3%, HMA_5%, and HMA_10% respectively. The standard deviations are reported as well.

The effect of the thickness and the overlap on the separation time was evaluated as well on the HMA_10%. Thus, SLJ tests were carried out for these joints configuration as well. Table 4 shows the maximum average loads for these different overlaps and thicknesses configurations.

The average maximum loads for the three different adhesive thicknesses are reported in Table 5. The average maximum load are 762 N (1.52 MPa), 881 N (1.79 MPa) respectively for 1.5 and 1.0 mm thicknesses. On the other hand, a substrate failure was observed in the SLJ specimens with a thickness of 0.5, with a maximum average load of 998 N (2.0 MPa). In this case, the used overlap length was 25 mm.

All the fracture surfaces of the SLJ specimens were evaluated after the test by means of visual inspection. Fig. 6 shows a representative fracture surface of HMA_5%. The red lines illustrate areas where the fracture was adhesive. In the rest, the separation was cohesive.

Fig. 7 displays representative fracture surfaces of HMA, HMA_3%, HMA_5% and HMA_10%. The cohesive areas are recognizable by the colours that are slightly clearer when compared to that where the separation was adhesive. Fig. 7 illustrates the nanoparticle introduction



**Fig. 5.** Representative curves of SLJ tests of the different adhesive compositions.

**Table 3**
Summary of the maximum adhesive loads and the relative shear strengths.

| | Pristine HMA | HMA_3% | HMA_5% | HMA_10% |
|---|---|---|---|---|
| Average maximum load (Shear strength) [N] | 835.55 (1.67) | 878.15 (1.75) | 881.45 (1.76) | 895.14 (1.79) |
| Standard Deviation [N] | 22.52 | 20.27 | 30.84 | 16.66 |
| Percentage increase [%] | – – | 5.10 | 5.50 | 7.20 |

**Table 4**
Summary of the maximum adhesive loads for three overlap configurations.

| Overlap | 12 mm | 18.5 mm | 25 mm |
|---|---|---|---|
| Average maximum load (Shear strength) [N] | 473 (1.97 MPa) | 668 (1.80 MPa) | 881 (1.76 MPa) |
| Standard Deviation [N] | 8.23 | 30.52 | 23.75 |

**Table 5**
Summary of the maximum adhesive loads for three overlap configurations.

| Thickness | 0.5 mm | 1.0 mm | 1.5 mm |
|---|---|---|---|
| Average maximum load (Shear strength) [N] | 998 N (2.0 MPa) | 881 (1.76 MPa) | 762 N (1.52 MPa) |
| Standard Deviation [N] | 9.42 | 23.75 | 14.01 |
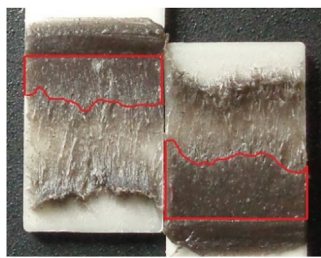


**Fig. 6.** Fracture surface of HMA_5%.

increases the size of the cohesive fracture area and it is worth noting that the size of cohesive fracture areas increases with the particle weight concentration. This leads to higher mechanical loads, as shown in Fig. 5 and Table 3.

Fig. 8 shows representative fracture surfaces of HMA_10% for three different adhesive thicknesses. The fracture surface related to the adhesive thickness of 0.5 mm presents a different fracture surface compared to all the others, since the deformation of the substrate was observed during the test. On the other hand, the fracture surfaces relater to 1.0 mm and 1.5 mm are very similar.

Fig. 9 displays representative fracture surfaces of HMA_10% for three different overlaps, namely 12, 18.5 and 25 mm. This figure shows that the cohesive area increases for lower overlap and that the adhesive fracture surface related to the overlap of 12 mm is mostly cohesive.

### 3.2. Sensitivity of nanomodified adhesive to electromagnetic parameters

#### 3.2.1. Applied current/power dependency

Fig. 10 shows the separation time (index of the time needed to reach the melt of the adhesive and the consecutive joint separation) as a function of the power intensity of the inductor for the HMA_5% and HMA_10%. This diagram shows the dependency of the separation time as a function of the applied current (I) and power. The currents and power values are reported in the x-axis of Fig. 10. The inductor displays the values of the power and the currents. For this test, the frequency is kept constant at 315 kHz. The test has been conducted with four different values of the requested currents (set point values) namely 300, 400, 450 and 550 A. However, the system is able to calculate the effective maximum current that circulates in the coil based on an internal algorithm that measure the reactive power. Thus, the effective currents that circulate in the coil are: 300, 400, 450 and 470 A. The power related to these currents are 3.4, 5.5, 6.6 and 7.0 kW, respectively. The coil voltage is 16 V. The results show that applying a current of 300 A, the time needed to separate the adherends bonded with HMA_10% is 27 s. Increasing the current value to 400 A the separation time is reduced to 15.1 s (nearly half of the time). By further increasing the current intensity up to 470 A, there is a further slight decrease of 1.1 s. While, from 300 to 400 A there is a consistent drop of the separation time the reduction is slight from 400 to 470 A, around 1.3 s. The current increase in the latter range seems to be less effective when the value of 400 A is overcome. These tests were conducted with a circular three-turn coil.

Fig. 10 shows the dependency of the current on the separation time for HMA_5% as well. In this graph, the power values below 400 A have not been reported because of the high value of the separation time compared to the higher powers, they were higher than 150 s. The tests have been conducted for three different currents, starting from a higher value with respect to what was done for the HMA_10% case, that are 400, 450 and 470 A. Fig. 10 shows that the trend of HMA_5% is similar to the HMA_10% and again the separation time decreases with current increase. Applying a current of 400 A, the time needed to separate the adherends is 68 s. Increasing the current to the maximum value, 470 A, the separation time is 42.9 s that corresponds to a reduction of the separation time of 25.1 s. A power increase from 6.6 to 7.8 kW leads to a reduction of the separation time of 5.9 s. As for the previous case, the adopted coil is the circular one and the value of the separation time tends to be similar when higher values of the current are applied. This analysis was not conducted for HMA_3% in weight because of the higher separation time and the consequently limited range of evaluation.

The values reported show that HMA_10% gives better results in
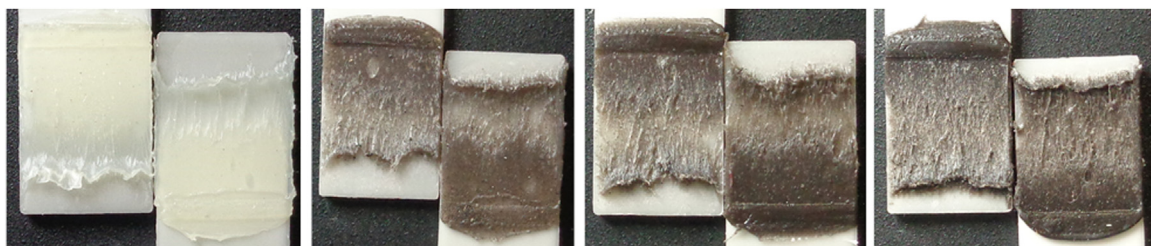


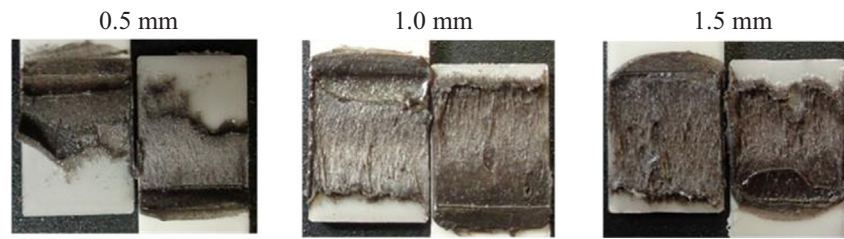**Fig. 7.** Representative fracture surfaces of HMA, HMA_3%, HMA_5% and HMA_10%.

**Fig. 8.** Representative fracture surfaces of HMA_10% for three different adhesive thicknesses.

terms of separation time, as expected. In the most cases, the separation time of HMA_10% is at least 70% lower than HMA_5%. The error bars in Fig. 10 report the values of the standard deviations of the separation time. As can be seen, the values of standard deviations are higher for the HMA_5%.

### 3.2.2. Frequency dependency

Fig. 11 shows the values of the separation time as a function of the frequency for HMA_10%, HMA_5% and HMA_3%. For this analysis, a circular coil shape was adopted. In this case, three different values of the frequency were considered. The value of the current for this investigation was set to 19.5 A, maximum value of the machine. The power decreases when frequency increases because of the modification of different parameters such as polarization peak, gauge, electrical conductivity and cross-sectional area, according to [21]. The reported values show that there is a high dependency of the separation time on the frequency. Despite the applied power reduction, resulting from the increase of the frequency, there is a reduction of the separation time, for HMA_10%, of 9 s changing from 209 to 244 kHz and further 7 s from 244 to 317 kHz. The trend of the separation time shows that it is possible to separate in less time, saving the input power just by increasing the frequency. Fig. 11 shows the values of the separation time as a function of the frequency for HMA_5% as well. These values are higher compared to the compound HMA_10%. The trend is almost the same: higher the frequency lower the separation time, despite the decrease of the applied power. It is important to note that in this case, the gap of the separation time between 209 kHz and 244 kHz is higher than the following, the gap between 244 kHz and 317 kHz. The difference in separation time between the first and the second value of the frequency is 10.58 s. The differences between the second and the third are 35.66 s.

The values of the separation time as a function of the frequency of HMA_3% are illustrated in Fig. 11 as well. These values are higher compared to the HMA_10% and HMA_5%. In this graph, the value at 207 kHz has not been reported because after 200 s no separation occurred. From 244 kHz to 317 kHz there is a drop of the separation time of 35.29 s. These analyses show that the frequency is a factor that highly influences the separation time. Error bars in Fig. 11 report the values of the standard deviations for all the three compounds. As can be noted, the values of the scatter are lower when frequency and particle concentrations are higher. The coil current in this case was 470 A.

### 3.2.3. Diameter and shape dependency

Figs. 12, 13 and 14 show the separation time of the two different coil shapes and for three different tube diameters of the coil. Every experimental test was done for the three different concentrations of iron
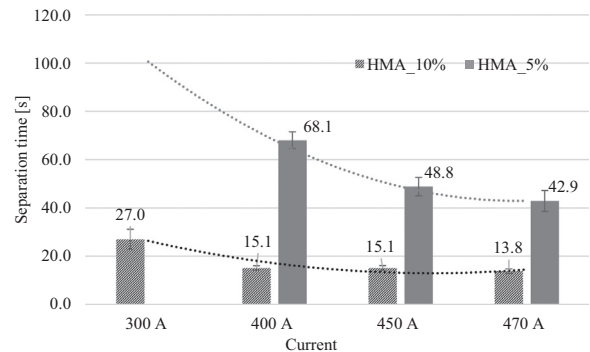


**Fig. 10.** Separation time as a function of the power for HMA_10% and HMA_5% at the frequency of 315 kHz.
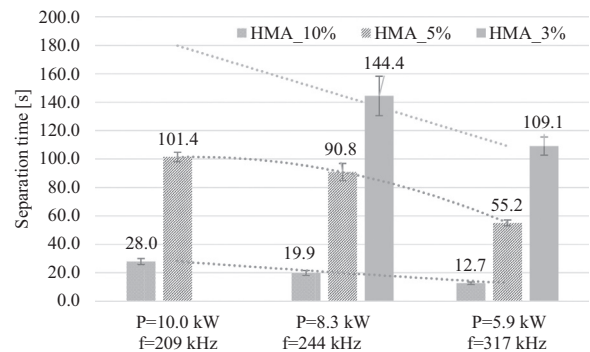


**Fig. 11.** Separation time as a function of the frequency for the HMA_3%, HMA_5%, and HMA_10%.

oxide. For this analysis, the value of the current used was 19.5 A.

The modification of the diameter of the coils is not possible without modifying the frequency, as motivated in Section 2. Furthermore, frequency depends on different factors (the shape of the coil, diameter, and length of the coil). For this reason, it was not possible to make coils that work exactly at the same frequency. Nevertheless, it was possible to limit the values of the frequency to a narrow range, around 20 kHz. When the frequency is modified, supply power changes as well, but it has a lower effect on separation time in the considered range, as shown in the "Applied current/power dependency" section. The values of the powers and the frequencies are reported in Table 6. The coil current in this case was 470 A.
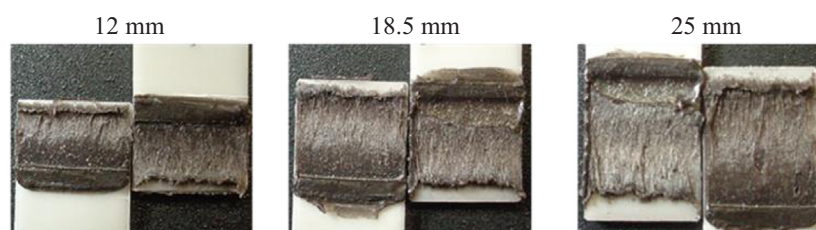


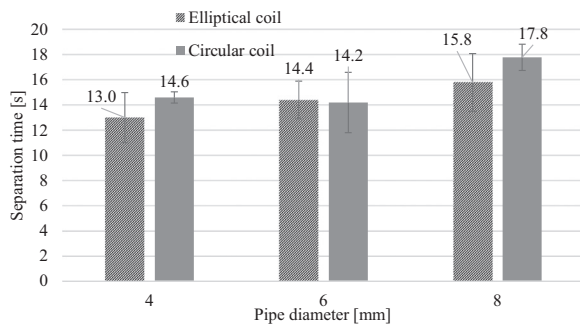**Fig. 9.** Representative fracture surfaces of HMA_10% for three different overlaps.

**Fig. 12.** Separation time as a function of the diameter for the HMA_10% for the circular (left bin) and elliptic (right bin) shape.
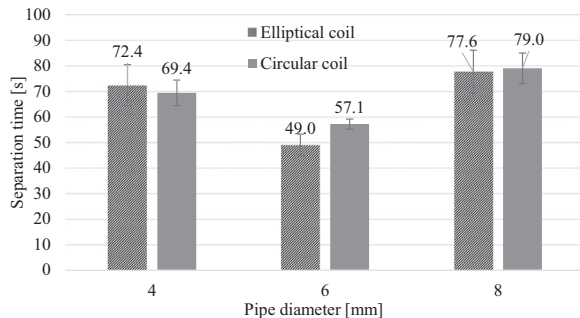


**Fig. 13.** Separation time as a function of the diameter for the HMA_5% for the circular (left bin) and elliptic (right bin) shape.
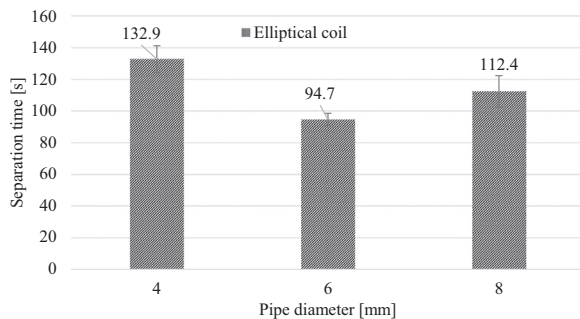


**Fig. 14.** Separation time as a function of the diameter for the HMA_3%.

**Table 6**
Values of the frequencies and powers for the different.

|  | Elliptical coil | Circular coil |
|---|---|---|
| 4 mm diameter pipe coil | 289 kHz–7.8 kW | 287 kHz–7.5 kW |
| 6 mm diameter pipe coil | 309 kHz–6.3 kW | 287 kHz–6.5 kW |
| 8 mm diameter pipe coil | 312 kHz–5.9 kW | 307 kHz–5.6 kW |

Fig. 12 reports the separation time as a function of the diameter for the circular shape coil (left bin) and the elliptical shape coil (right bin). In this Figure, the concentration of iron oxide in the adhesive matrix is 10% in weight. The values of the separation time are very close to both the circular shape and the elliptical shape. Concerning the circular shape, the values of the separation time are almost the same in the case of a 6 mm pipe coil. On the other hand, the time is lower for the elliptic coil in the case of 4 and 8 mm pipe coils. In fact, the difference in the separation time for the elliptic shape is respectively 1.6 s and 2 s less than the circular ones. This could mean that, for this particular case, the closeness of the tube to the adhesive layer could be an influencing parameter. In this perspective, we have to take into account that the frequency is a little bit higher for the elliptical 6 mm coil and this

parameter could influence the results. In general, the values related to 4 and 6 mm diameters are lower compared to the 8 mm diameters, even though, in this case, the frequency is higher.

Fig. 13 shows the trends of the separation time as a function of the diameter for HMA_5%. These values are significantly higher than the separation times of the HMA_10%. The times needed to separate the joints for the elliptically shaped coil are 4, 8 and 43 s respectively lower than those for the circular shaped one, respectively for the 4, 6 and 8 mm diameter tubes. The trends are similar for the two different coil shapes. The lowest value of the separation time is when a coil with a diameter of 6 mm is used while the other values at different diameters are higher.

Fig. 14 shows the values of the separation time as a function of the tube diameters for the elliptical coil. The values of the circular coils are not reported because no separations occurred after 160 s of induction heating. The trend is similar to the HMA_5%, with the separation time that is lower using a tube diameter of 6 mm while it is higher for the other two diameters. It should be noticed that the separation times increased approximately by a factor of 2 with this reduction in the iron oxide percentage. The exception with this compound, compared to the HMA_5% and HMA_10%, is that the separation time for the tube diameter of 4 mm is higher than the separation time for the 8 mm tube diameter.

It is noticeable that the separation time is highly influenced by the particles concentration. Considering the lowest values of the separation time for the elliptically shaped coil with a tube diameter of 6 mm, there is an increase of 35 seconds passing from HMA_10% to HMA_5% and 45 seconds from HMA_5% to HMA_3%. The difference in the separation time is even higher for the other tube diameters.

The separation values are very close passing from 4 to 8 mm for HMA_10%, this gap is much higher for HMA_5% and HMA_3%. The analysis showed that the closeness (the difference between circular and elliptic coil) of the coil to the workpiece is an influencing factor. Furthermore, the coil temperature was monitored as well by the IR-camera. The coil temperatures of the 6 and 8 mm pipe coils were similar and they reached a maximum temperature of 42 °C in the case of the higher separation times. On the other hand, the 4 mm pipe coil reached a maximum temperature of 80 °C, for the higher separation time as well. This temperature is not significantly higher than the previous one but the results were surprisingly different. This could be due to two reasons. The first one could be due to the small variations of the applied power and frequency that are different for the two coils and diameters. The second one could be due to the different particle distribution inside the adhesive matrix for HMA_10%, HMA_5% and HMA_3%. As shown in the SEM analysis section, the particles distribution is more uniform in the HMA_10% due to the higher weight fraction of particles. On the other hand, as expected, HMA_5% and HMA_3% showed some areas with a lack of particles since the weight concentration was lower. These richer areas could be distributed in a different part of the adhesive volume that could be able to heat the adhesive in a more efficient way. This behaviour could lead to the higher scatter and the unexpected result showed in this section. Figs. 12, 13 and 14 report the values of the standard deviation in the error bars.

### 3.2.4. Pancake coil

Fig. 15 shows the values of the separation time using a pancake coil. The pancake coil is a three-turn coil with a tube diameter of 4 mm since it was easier to fabricate. As in the previous cases, the higher particles concentrations lower the separation time. As can be seen, the values for the pancake coil are higher compared to the values of the elliptical coils presented in the previous section. The separation time is 20 s for HMA_3%, 16 s higher for HMA_5% and 7 s higher using HMA_10%. However, it should be taken into account that the frequency (that is a high influencing parameter) is 34 kHz lower if compared to that used in the previous section. The coil current in this case was 470 A.
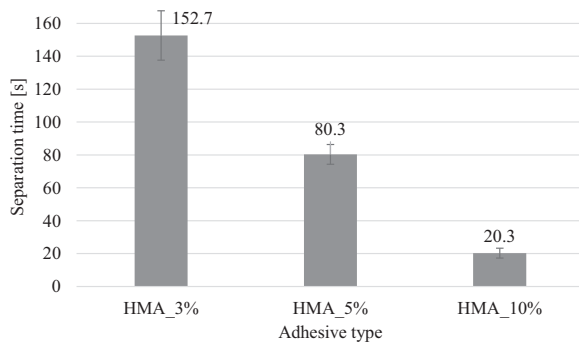
**Fig. 15.** Separation time of the pancake coil of the three different compounds.

### 3.2.5. Disassembled surfaces

Fig. 16 shows representative surfaces of disbonded joints prepared with HMA_3%, HMA_5%, and HMA_10%. All the surface separations are cohesive and similar, as expected. The colours of the adhesives are darker for the adhesive with a higher particles concentration. Further, there are brighter spots on the left side of the separation surfaces of HMA_5% and HMA_10% that are the part where the HMA starts to melt.

### 3.2.6. Temperature curves of nanomodified adhesive under induction heating

Experimental tests showed that the temperature-time curves recorded on the edge of the single lap joint specimen were very similar to the ones recorded on the adhesive layer alone. Fig. 17 shows the experimental set-up in the case of the test on the adhesive layer.

Fig. 18 shows the temperature-time curves recorded directly on the adhesive layer and the adhesive edge of the SLJ. The curves show that there is no significant difference between the curves of the SLJ and on the adhesive layer. Furthermore, the authors measured average time to reach 135 °C (separation temperature by using the mass of 0.5 kg). These average time were 13.6 s (Standard deviation 1.5 s) in the case of the SLJ and 13.2 s (Standard deviation 0.9 s) in the case of the adhesive layer. For this reason, all the temperatures reported in this work refer to the ones measured on the edge of the SLJ.

Fig. 19 illustrates the temperature profiles of the modified adhesive during the electromagnetic joint separations for HMA_3%, HMA_5%, and HMA_10%. The Figure shows the heating process of the adhesive monitored with a IR camera. The IR camera was calibrated by using a thermocouple and a hot plate in order to prevent eventual errors due to the adhesive emissivity change. The black line marks the point where the separation started with the slide of the lower substrate that is loaded with a weight of 0.5 N. As expected and as shown in the reported separation time diagrams, the HMA_10% has the more rapid heating while HMA_5% and HMA_3% heating is lower. After the sliding of the temperature increases since the central parts of the adhesive showed up and are hotter than the temperature measured on the edge. The maximum observed temperature during this test was 168 °C that is still far from the initial thermal degradation temperature.

The heating process can be divided into four different steps that are illustrated in Fig. 20. In the first one, the temperature of the modified



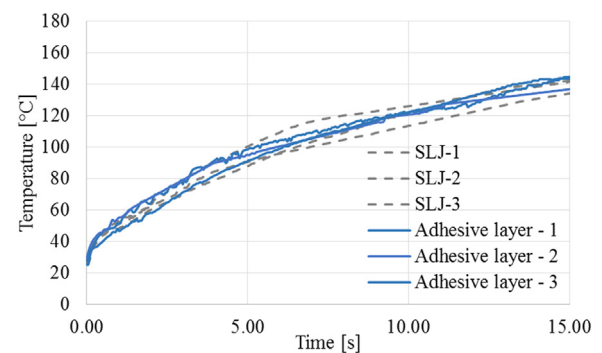**Fig. 17.** Experimental set-up of the temperature measurement.



**Fig. 18.** Temperature-time curves measured on adhesive layers and SLJ edges.
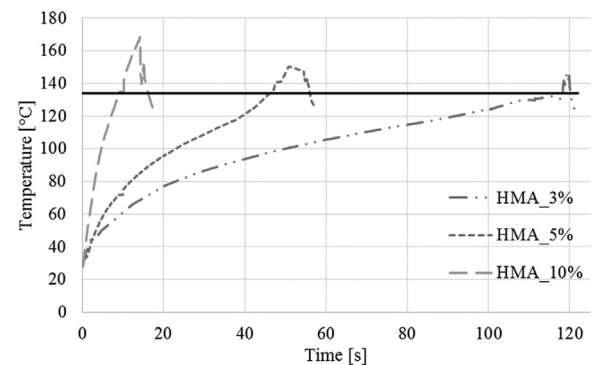


**Fig. 19.** Temperature profile over the time for SLJs, monitored with IR camera.

adhesive starts to increase. In the second and third ones, the adhesive temperature continues to rise and the substrate temperature starts to increase for conduction. In the last picture, the adhesive overcomes
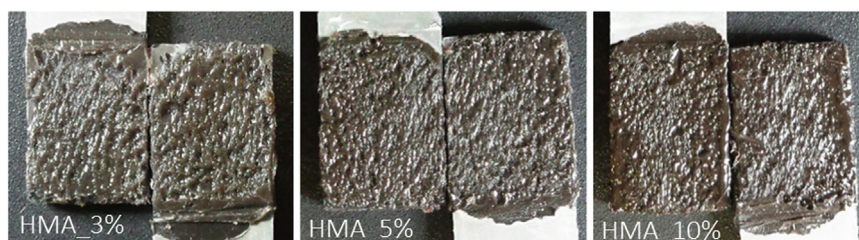


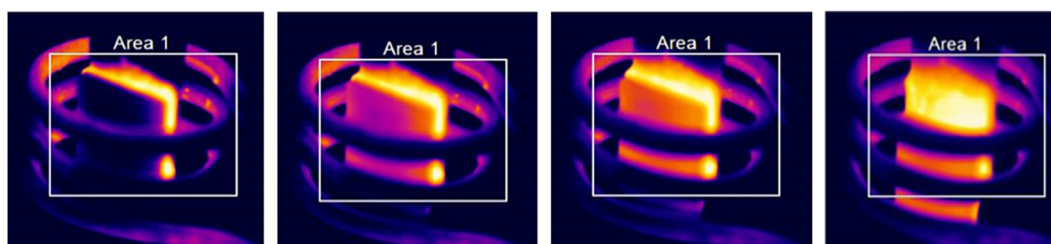**Fig. 16.** Representative surfaces of HMA_3%, HMA_5% and HMA_10% after the induction heating separation.
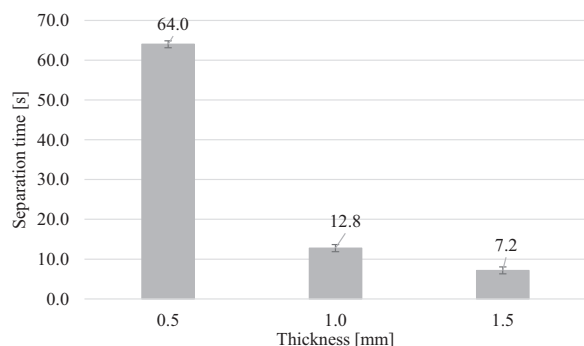
**Fig. 20.** Thermal images of the separation process.



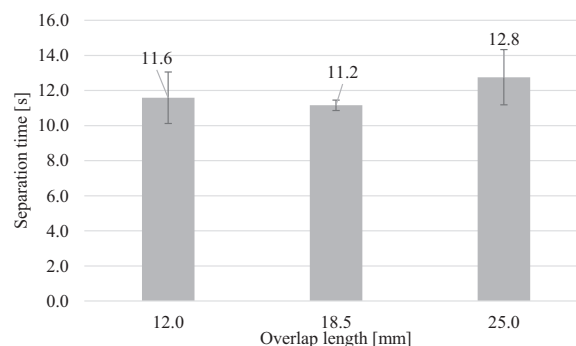**Fig. 21.** Effect of the adhesive thickness on the separation time.



**Fig. 23.** Effect of the adhesive overlap on the separation time.

135 °C and the substrate starts to slide and reveal the internal temperature, 160 °C, of the adhesive that is higher than that recorded one on the joint edge. In fact, the diagram of Fig. 16 shows that, after the sliding temperature is overcome, the temperatures rise. These temperatures are the temperatures of the internal part of the joint that overcome the melting temperature of the adhesive. The thickness of the adhesive presented in Fig. 20 is 1.0 mm and the overlap is 25 mm.

Fig. 21 shows the values of the separation time for three different thicknesses of the adhesive layer: 0.5, 1.0 and 1.5 mm. In these cases, the overlap length is 25 mm. Fig. 21 reveals that there is a marked drop of the separation time for higher thicknesses. The values of the separation time with the thickness of 0.5 mm is unexpectedly higher. The reduction of the separation time is around 80% for the adhesive joint with 1.0 mm thickness and 90% for the adhesive joint with 1.5 mm thickness. Fig. 21 reports error bars of the separation time values as well.

The analysis of the IR camera (IRtech radiamatic Timage) showed that heat is absorbed by the substrates in the adhesive joints with a smaller thickness. The temperature of the substrate Fig. 22 illustrates the temperatures of the adhesive substrates when the adhesive temperature is 130 °C, which is the initial sliding temperature of the lower surface, as described above. As shown in Fig. 22, the substrate temperature of the adhesive joint with a thickness of 0.5 mm is 40 °C. On the other hand, the substrate temperatures, at the same time, for the adhesive joints with a thickness of 1.0 and 1.5 mm is 30 °C. This means that for lower adhesive thickness the substrates absorb small thermal energy in this phase.

Fig. 23 shows the values of the separation time for three different overlap lengths of the adhesive layer: 12, 18.5 and 25 mm. In these cases, the adhesive thickness is 1 mm. Fig. 23 displays that there is no a significant difference of the separation time with the overlap length.

Fig. 24 shows the substrate temperature of the three adhesive joint an instant before the sliding starts. While the substrate temperature of the bonded joints of the 1.0 and 1.5 mm adhesive joints is close to the starting point 27 °C, the substrate temperature of 0.5 mm adhesive joint is 90 °C. This means that the substrates related to the smallest thickness absorb more thermal energy compared to the thicker ones. This could be linked to the higher interfacial strength of the adhesive joint with a thickness of 0.5 mm, as shown at the beginning of this section. In this case, the small weight used for initiating the slide of the lower substrate was not enough and thus did not slide due to the substrates absorbing the thermal energy up to the point where the adhesive had completed melted and finally separated. This behaviour explains the higher separation time as well.

### 3.3. Scanning electron microscope analysis

SEM analysis was used in order to investigate the general distribution of the particles within the adhesive. Fig. 25 shows a representative SEM image at 500× magnification of the nanomodified adhesive HMA_10%. As illustrated in Fig. 25, the tiny white spots are the iron oxide nanoparticles embedded in the HMA matrix. The distribution of the nanofiller in the matrix seems to be quite uniform in the matrix.

The presence of nanoparticles is investigated at higher magnification as well. Figs. 26a and 26b show SEM images of the modified adhesive at 5000× and at 10000×, respectively. Fig. 26 shows that
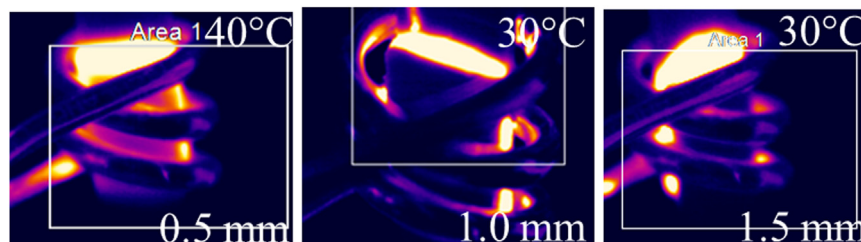


**Fig. 22.** Substrate temperature when the adhesive temperature is 130 °C (initial sliding temperature).
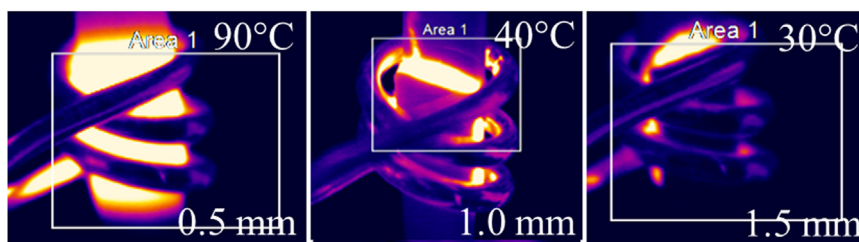
**Fig. 24.** Substrate temperature of the three adhesive joint thickness before the sliding of the lower substrate.
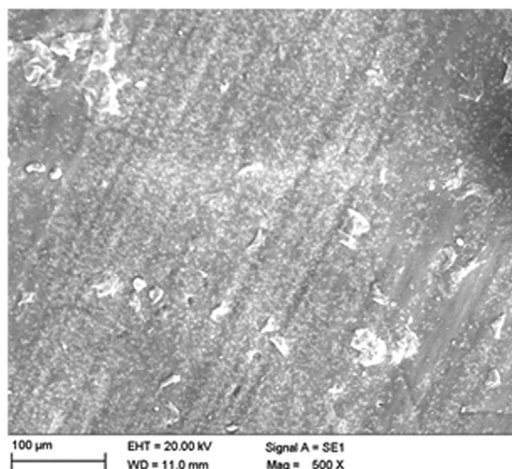


**Fig. 25.** Representative SEM image at 500× of HMA_10%.

nanoparticles tend to form agglomerates with limited size (about 1 μm). The presence of these small aggregates is attributed to the nature of the particles that, before mixing, display a tendency to agglomerate as shown in [19] with AFM microscopy. AFM evidenced that the dimension of a single particle is lower than 55 nm, but the particles aggregate as clusters with size very close to the one measured in the adhesive matrix. The lowest cluster length is around 0.78 μm.

Fig. 27 shows the dispersion of the HMA_5%. Fig. 27a shows that the presence of the nanofiller is lower compared to HMA_10%. There are some areas where there is no presence of iron oxide, such as the upper left and the lower right corners of Fig. 27b. The higher magnification image, Fig. 27b, shows that there is no formation of big agglomerates, as illustrated for HMA_10%. In fact, the size of the iron oxide clusters is lower than the 1 μm scale.

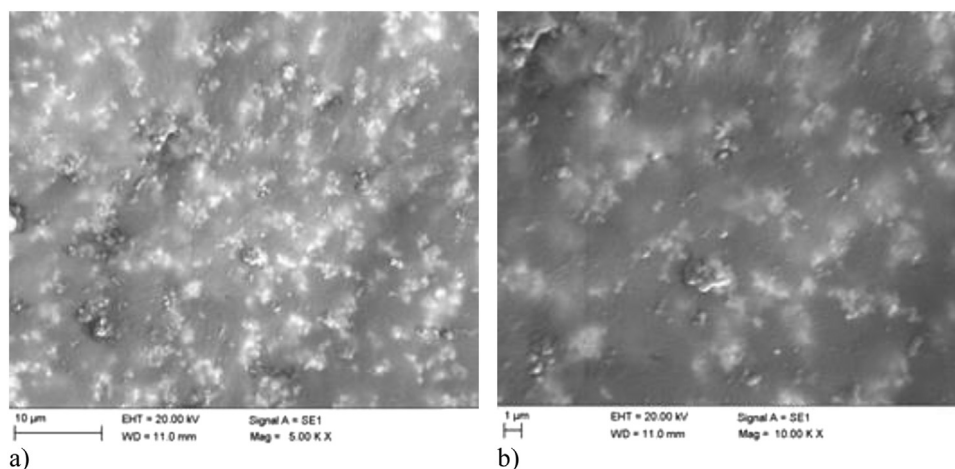Fig. 28 illustrates a SEM magnification of the HMA_3% at 10000×.

As expected, the particles distribution results similar to the HMA_5%.

### 3.4. Thermogravimetric analysis

Thermogravimetric analysis (TGA) is carried out in order to understand whether the concentration of the nanofiller is correct and in order to verify if after induction heating process the polymer begins to degrade. Therefore, the TGA of the pristine adhesive has been correlated with the TGA curves of HMA_3%, HMA_5% and HMA_10% after the separation with the induction heating process.

Fig. 29 shows the representative TGA curves for the pristine HMA (so without induction heating process), HMA_3%, HMA_5% and HMA_10% after the induction heating process. The four curves are almost superimposed except for the final part where the concentration is higher based on the particle concentration of the adhesive. This means that the two samples are subjected to the same degradation process, as expected. The motivation is due to the fact that the temperature of the separation process does not overcome 160 °C and TGA results showed that the degradation point of this adhesive is around 230 °C. The final weight concentrations are not exactly 3%, 5%, and 10% but the average over three replication is respectively 3.62%, 5.87% and 10.45%.

### 4. Conclusions

This work reports experimental results of a study on a technology able to separate nanomodified hot-melt adhesives with iron oxide particles by mean of electromagnetic fields. The aim of this study was to understand whether the use of this compound, coupled with electromagnetic induction, is able to obtain the separation of the two substrates in a relatively short time. Furthermore, the objective was to clarify which are the most influencing parameters for this application.

The parameters analysed in this experimental activity are the shape of the coil, the frequency of the generator, the circulating currents and the diameter of the pipe coil. The separation tests with different diameters of the pipe coil were carried out to assess whether the different
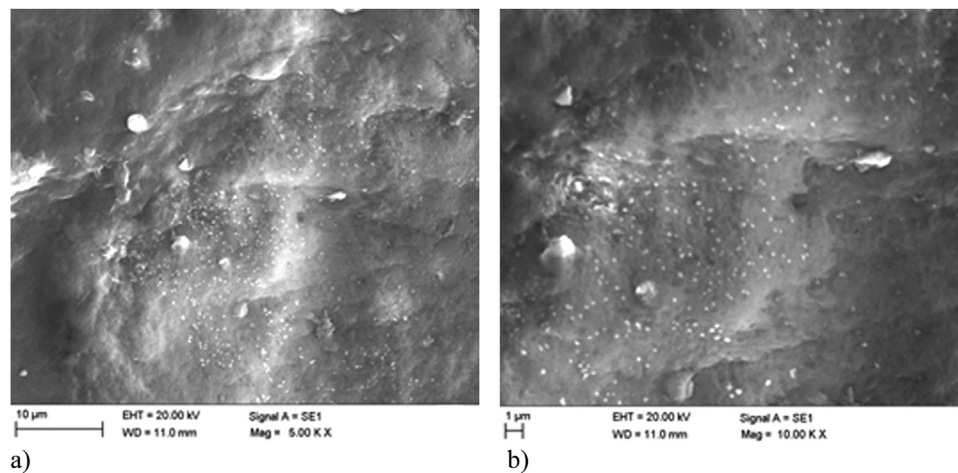


**Fig. 26.** SEM images of HMA_10%: a) 5000×; b) 10000×.
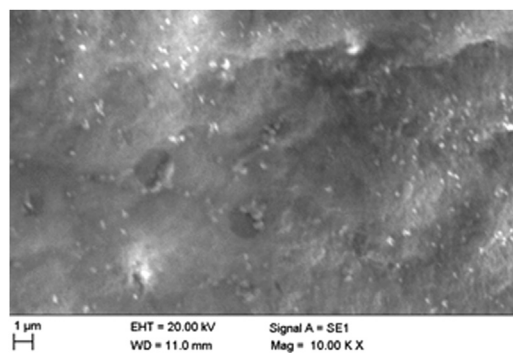
**Fig. 27.** SEM images of HMA_5%: a) 5000×; b) 10000×.



**Fig. 28.** SEM images of HMA_3%. 10000×.

diameter of the pipe coil, linked to the water mass flow and to the coil temperature can affect the separation process. The sensitivity of these parameters was assessed by mean of the separation time that is the time needed to heat the adhesive up and the consecutive separation. Based on the experimental results, the following conclusions can be drown:

- Mechanical test carried out on Single Lap Joint specimens showed that ultimate loads increases by the particle concentration. The maximum load of HMA_10% was found to be 7% higher than the pristine adhesive while HMA_3% and 5% were 5% higher than the pristine one. Furthermore, nanomodified adhesives presented higher elongations of the pristine adhesive.

- Experimental separation tests showed that the increase of the frequency contributes to lower the separation time. It has been found that increasing the frequency of 103 kHz, from 209 to 312 kHz, can halve the values of the separation time for HMA_10% and HMA_5%. The applied current influences the separation process as well but especially in a low range. The influence seems to be lower when the current increases, especially in the interval 400–470 A where the values tend to be very similar.

- Separation tests conducted on pancake coil showed that separation is possible with this coil but in shorter time even though this could be connected to the lower value of the frequency that this coil has.

- The analysis showed that the closeness (the difference between circular and elliptic coil) of the coil to the workpiece is an influencing factor as well. On the other hand, the change of the diameter of the pipe coil did not influence a lot the temperature and the separation time. The coil temperatures of the 6 and 8 mm pipe coils were similar and they reached a maximum temperature of 42 °C in the case of the higher separation times. On the other hand, the 4 mm pipe coil reached a maximum temperature of 80 °C, for the higher separation time as well. This temperature is not significantly higher than the previous one but the results were surprisingly different. This could be due to small variations of the applied power and frequency that are different for the six fabricated coils or, as well, to the diverse distribution of the particles inside the adhesive matrix, especially for the lower concentrations. Generally, the adhesives modified with lower particle concentrations have a lower number of
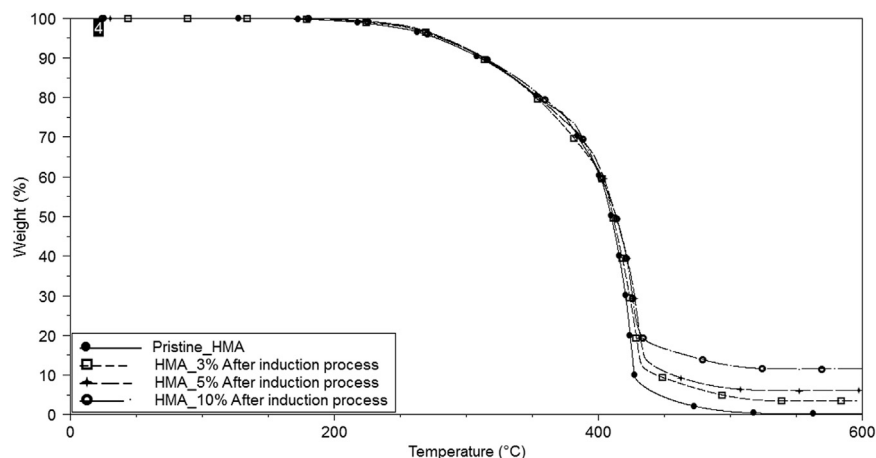


**Fig. 29.** TGA of the pristine HMA and HMA_3%, HMA_5% and HMA_10% after the induction.

particles and so the possibility to have some areas richer than others is higher than that with a higher particles concentration. This could also explain why adhesive modified with lower particles concentrations have higher scatters.

- Separation tests conducted on the different overlap lengths showed that there is no significant difference among separation time. On the other hand, separation tests conducted on the different thickness showed that the separation time increase with lower thickness. The separation time of the joint with a thickness of 0.5 mm is five times higher compared to the joint with a thickness of 1.0 mm. Although the recommended adhesive thickness for this adhesive is 1.0 mm there is a limitation for the applications that requires lower adhesive thicknesses.

- The separation surfaces of mechanical and electromagnetic induction tests were analysed by visual inspection. The separation surfaces after the electromagnetic induction for all the specimens were totally cohesive, differently by the mechanical tests where a small part was adhesive and the bigger parts were cohesive. This analysis showed that the electromagnetic separation occurs only when the adhesive is melted.

- Separation tests conducted on different adhesive joint thicknesses showed that the separation time is higher for joints prepared with smaller adhesive thicknesses. This could be due to the higher adhesive strength of the joint with an adhesive thickness of 0.5 mm. In this case, the small weight used for initiating the slide of the lower substrate could not be enough and thus the slide does not start and substrates absorb thermal energy up to the complete adhesive melting and the consecutive separation.

- Scanning electron microscope reveals the presence of some nanoparticle clusters that tend to agglomerate especially in HMA_10%. In HMA_3% and HMA_5%, particles are visible only in small areas due to the lower particle numbers present into the matrix.

- The thermo-gravimetric analysis shows that the weight-temperature curves are almost superimposed both for HMA_3%, HMA_5% and HMA_10%. This proves that the induction heating process does not degrade the adhesive. For this reason, these adhesives can be reused in order to separate the substrates when needed.

This preliminary experimental activity carried out in this work showed that the separation of SLJ is possible by using this technique. The analysis showed that the lowest separation time was obtained with a frequency of 317 kHz and a current of 470 A when using a circular coil. For this reason, small coils could be used for small components such as lamp housing and air ducts. On the other hand, the possibility to bond or disassemble large plastic component, such as bumper or low tail gate, should be designed properly by taking in account that high frequencies are able to separate in lower time. Pancake coils can be used for this purpose but two or more inductors should be used in order to obtain a relatively rapid bonding.

## References

[1] Chang B, Shi Y, Dong S. Comparative studies on stresses in weld-bonded, spot-welded and adhesive-bonded joints. J Mater Process Technol 1999;87:230–6.

[2] Belingardi G, Chiandussi G. Stress flow in thin walled box beams obtained by adhesive bonding joining technology. Int J Adhes Adhes 2004;24:423–39.

[3] Belingardi G, Brunella V, Martorana B, Ciardiello R. Thermoplastic adhesive for automotive applications. In: Rudawska A, editor. Adhesive – application and properties Rijeka. Rijeka (HR): INTECH; 2016. p. 341–62.

[4] Casalegno V, Salvo M, Rizzo S, Goglio L, Damiano O, Ferraris M. Joining of carbon fibre reinforced polymer to Al-Si alloy for space applications. Int J Adhes Adhes 2018;82:146–52.

[5] Lu Y, Broughton J, Winfield P. A review of innovations in disbonding techniques for repair and recycling of automotive vehicles. Int J Adhes Adhes 2014;59:119–27.

[6] Verna E, Cannavaro I, Brunella V, Koricho EG, Belingardi G, Roncato D, et al. Adhesive joining technologies activated by electro-magnetic external trims. Int J Adhes Adhes 2013;46:21–5.

[7] Banea M, da Silva, Carbas R. Debonding on command of adhesive joints for the automotive industry. Int J Adhes Adhes 2015;59:14–20.

[8] Ciardiello R, Martorana B, Lambertini VG, Brunella V. Iron-based reversible adhesives: effect of particles size on mechanical properties. Proc Inst Mech Eng C 2018;232(8):1446–55.

[9] Severijns C, Teixeira de Freitas S, Poulis JA. Susceptor-assisted induction curing behaviour of a two component epoxy paste adhesive for aerospace applications. Int J Adhes Adhes 2017;75:155–64.

[10] Jeun M, Lee S, Kang JK, Tomitaka A, Kang KW, Kim Y, et al. Physical limits of pure superparamagnetic $Fe_3O_4$ nanoparticles for a local hyperthermia agent in nanomedicine. Appl Phys Lett 2012;100:406–11.

[11] Ghazanfari M, Kashefi M, Shams S, Jaafari M. Perspective of $Fe_3O_4$ nanoparticles role in biomedical applications. Biochem Res Int 2016. https://doi.org/10.1155/2016/7840161. [Article ID 7840161, 32 pages].

[12] Moskowitz BM, Frankel RB, Walton S, Dickson DPE, Wong KKW, Douglas T, et al. Determination of the preexponential frequency factor for superparamagnetic maghemite particles in magnetoferritin. J Geophys Res 1997;102(97):226–671.

[13] Kandasamy G, Maity D. Recent advances in superparamagnetic iron oxide nanoparticles (SPIONs) for in vitro and in vivo cancer nanotheranostics. Int J Pharm 2015;496:191–218.

[14] Haimbaugh R. Practical induction heat treating. 1st ed Ohio: ASM International; 2001.

[15] Rudnev V, Loveless D, Cook R, Black M. Handbook of induction heating.. 1st ed New York: Dekker Inc; 2003.

[16] Verna E, Koricho E, Spezzati G, Belingardi G, Martorana B, Roncato D, et al. Brunella Validation of a new nano-modified adhesive joining technology triggered by electromagnetic field, by testing of a real component In: Proceedings of the European conference on composite materials ECCM, Seville (Spain): 2014. pp. 22–26.

[17] Koricho E, Verna E, Belingardi G, Martorana B, Brunella V. Parametric study of hot-melt adhesive under accelerated ageing for automotive applications. Int J Adhes Adhes 2016;68:164–81.

[18] Ciardiello R, Belingardi G, Martorana B, Brunella V. A study of physical and mechanical properties of a nanomodified thermoplastic adhesive in normal and accelerated ageing conditions. In: Proceedings of the European conference on composite materials ECCM, Munich, Germany: 2016. pp. 26–30.

[19] Ciardiello R, Tridello A, Brunella V, Martorana B, Paolino DS, Belingardi G. Impact response of adhesive reversible joints made of thermoplastic nanomodified adhesive. J Adhes 2017;94:1051–66.

[20] Zhai L, Ling G, Li J, Wang Y. The effect of nanoparticles on the adhesion of epoxy adhesive. Mater Lett 2006;60:3031–3.

[21] Broddefalk A, Lindenmo M. Dependence of the power losses of a non-oriented 3% Si-steel on frequency and gauge. J Magn Magn Mater 2006;304:586–8.